The Chemostat Reactor: a Stability Analysis and Model Predictive Control

Guilherme Ozorio Cassol[a], Charles Robert Koch[b], Stevan Dubljevic[a]

[a] *Chemical and Materials Engineering Department*
University of Alberta, Edmonton
Alberta, Canada T6G 2V4
[b] *Mechanical Engineering Department*
University of Alberta, Edmonton
Alberta, Canada T6G 2V4

Abstract

The model predictive control of an unstable chemostat reactor is developed in this contribution. First, the system's model, a nonlinear first-order hyperbolic partial integro-differential equation (PIDE), is analyzed. and model linearization is considered around the unstable operating condition. The structure-preserving Cayley–Tustin transformation is used to obtain a discrete-time model representation of the system. Then, the operator Ricatti equations are solved in the discrete-time setting to obtain a full state feedback controller that stabilizes the closed-loop and design a Luenberger observer responsible for the state reconstruction. Finally, a dual-mode MPC is derived to guarantee constraints satisfaction and optimality, considering the gain-based unconstrained full-state feedback optimal control. This dual-mode approach leads to an optimization problem where the predictive controller only needs to make an action if the constraints are active in the control horizon. The results from simulation studies show the controller's performance.

Keywords: Model Predictive Control, Distributed Parameters System, Chemostat Reactor, Population Balance

Introduction

Chemostat reactors are essential in environmental research as they allow observing natural processes on a small scale [1]. They are also helpful in increasing the production rates of organisms that synthesize yeast or antibiotics, for example. While the biomass and the nutrient solution are mixed inside the chemostat reactor; the temperature, pH value, and volume of the liquid inside are kept constant under constant mixing, as represented in Figure 1. The inlet solution contains the nutrient solution, while the outlet is assumed to have the same composition as the liquid inside. The manipulated variable generally considered are the inlet and outlet flow rates. Given that inlet flow only contains the nutrient solution, an increase in the flow rate would lead to the dilution of the biomass inside [2].

*Corresponding author
Email address: Stevan.Dubljevic@ualberta.ca. (Stevan Dubljevic)

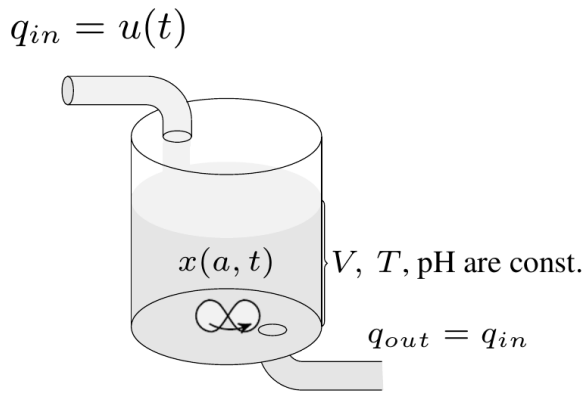

Figure 1: Chemostat reactor representation.

Describing population processes by age-structured models is a well-known approach [3]. Generally, these models do not consider self-competition, which increases the complexity of this control problem. If self-competition is assumed, the population dynamics inside the reactor is described by a nonlinear first-order hyperbolic partial integro-differential equation (PIDE) with integral boundary conditions.

The controller design for PIDEs has been the objective of many studies. One approach involves using spatial discretization techniques, thus converting the partial differential equations to sets of ordinary differential equations (ODEs) [4]. Then, the lumped model is used in the controller's synthesis, following the same strategies used for general finite dimensional systems. However, a problem arises with the number of modes that must be used to reach adequate model approximation. This results in high-order controllers, which are difficult to be conceived in practice [5, 6]. Another approach is to consider the infinite dimensionality of the PDEs in the controller design. Several contributions addressed the control problem by applying different methodologies, such as backstepping techniques, approximate inertial manifolds, robust control, and linear quadratic control in the frequency domain, to name a few [7, 8, 9, 10].

Specifically for age-structured population dynamics, the feedback control without considering the self-competition (without the integral term) has been studied in many past contributions. In [11], a feedback controller, which only needs output sampled data to track a reference trajectory, was considered. In [12], a tracking controller realization based on the decomposition of the PDE into a finite and an infinite dimensional part is considered. In addition, as shown in [13], it is possible to convert a first-order hyperbolic PIDE without self-competition into an ordinary integral delay equation for the design of the feedback controller.

System stabilization and output tracking are generally the main concerns in the realm of contributions found in the literature. However, there are only a few contributions where input and state constraints are considered. The model predictive control (MPC) can address the system stabilization while still optimizing the performance of a system subjected to constraints [14]. There are a few contributions aimed at the design of MPC controllers for PDEs using different methods, such as spatial discretization, controller design for

a class of the Riesz spectral systems with separable spectrum and piece-wise predictive feedback control [15, 16, 17]. This contribution uses a discrete-time representation of the system to implement the MPC. The Cayley-Tustin time discretization is considered, which uses the Crank-Nicolson midpoint integration rule and is easily applied in infinite-dimensional setting [18]. This scheme has been shown to preserve the intrinsic energy and dynamical properties of the linear distributed parameter system [19].

As the control of the chemostat reactor can result in higher production, in this contribution, the Model Predictive Control (MPC) is developed for such a system. The self-competition term is considered, and the model is linearized around the operating steady state. The stability analysis of the possible steady-states is then carried out. The linearized model around the desired steady-state is used to generate a discrete representation of the system using Cayley-Tustin, preserving the infinite-dimensional nature of the distributed parameter system. Then, the dual-mode MPC is derived. This type of controller can be used to optimize the performance of a system subjected to constraints. Differently from previous contributions [20, 21], the dual-mode considers a state-feedback law that guarantees closed-loop stability. Thus, the MPC controller only needs to take action when the constraints are active. Furthermore, as the MPC requires full state feedback and only the total amount of microorganisms in the reactor is available for measurement, a Luenberger observer design is also addressed. The operator Ricatti equation is solved in the discrete-time setting to guarantee the system's state reconstruction. Finally, the results from simulation studies show the controller's performance.

The contribution is organized as follows. First, the non-linear model representing the microorganism growth inside the Chemostat reactor is presented. The steady-state analysis for a given operating condition is derived in the following section. Then, a parameter continuation method is applied to the model, allowing the analysis of the effect of the system's parameter on the steady-states. Linearization and stability analysis are carried out in the subsequent sections. A full-state feedback control law and Luenberger observer gain are obtained with the linearized model by solving the related Ricatti equations. Then, the dual-mode MPC is derived based on the full-state feedback control law, guaranteeing the satisfaction of the imposed constraints. Finally, the simulation results show the system observer and MPC performance.

The Chesmostat Reactor

$$\begin{aligned} \frac{\partial x}{\partial t} &= -\frac{\partial x}{\partial a} - x\left[\mu(a) + u(t) + \int_0^W p(\alpha)x(t,\alpha)d\alpha\right] \\ x(t,0) &= \int_0^W k(\alpha)x(t,\alpha)d\alpha \\ y(t) &= \int_0^W x(t,\alpha)d\alpha \end{aligned} \tag{1}$$

with an initial condition (initial age profile) $x(0,a) = x_0(a) \in X$, where X is a real Hilbert space $L_2(0,W)$ and W is the maximum age considered. The positive state $x(a,t)$ describes the amount of microorganisms of a certain age at a specific time, with the mortality rate represented by the function $\mu(a)$. The self-competition

is described via an integral with integral kernel $p(a)$. The boundary condition is also an integral operator (with an integral kernel $k(a)$) that defines the birth rate of the youngest age microorganisms. The system's input is the bounded function $u(t)$, related to the dilution rate of the reactor. Due to the negative sign in the PIDE, a higher dilution reduces the concentration of the microorganisms, as one would expect. For physical reasons, the input is limited to a positive interval. The output $y(t)$ is the total amount of microorganisms in the reactor.

Steady-States

To determine the equilibrium profile, the following system of equations must be solved:

$$\begin{aligned} \frac{dx_{SS}}{da} &= -x_{SS}\left[\mu(a) + u_{SS} + \int_0^W p(\alpha)x_{SS}(\alpha)d\alpha\right] \\ x_{SS}(0) &= \int_0^W k(\alpha)x_{SS}(\alpha)d\alpha \\ y_{SS} &= \int_0^W x_{SS}(\alpha)d\alpha \end{aligned} \tag{2}$$

It is simple to see that this non-linear equation will always admit the trivial solution:

$$x_{SS}(a) = 0, \forall\, a \tag{3}$$

The other possible set of solutions of this non-linear integro ordinary differential equation can be achieved by setting:

$$u_{SS} + \int_0^W p(\alpha)x_{SS}(\alpha)d\alpha = \epsilon \tag{4}$$

and, by dividing both sides of Eq. 2 by x_{SS}, the equation becomes:

$$\frac{1}{x_{SS}}\frac{dx_{SS}}{da} = \frac{d[\ln x_{SS}]}{da} = -\left[\mu(a) + \epsilon\right] \tag{5}$$

which can be easily solved, resulting in the following expression:

$$x_{SS}(a) = x_{SS}(0)\mathrm{e}^{-\epsilon a - \int_0^W \mu(\alpha)d\alpha} \tag{6}$$

Finally, by applying the boundary condition, the following non-linear equation is obtained:

$$1 = \int_0^W k(\alpha)\mathrm{e}^{-\epsilon\alpha - \int_0^\alpha \mu(\beta)d\beta}d\alpha \tag{7}$$

In this equation, the only unknown is ϵ, as $k(a)$ and $\mu(a)$ are defined functions. If only physically meaningful steady-states are considered, $x_{SS}(a)$, defined in Eq. 6, should be a real-valued function. Thus, ϵ needs to be a real constant as well, making $\mathrm{e}^{\epsilon\alpha - \int_0^\alpha \mu(\beta)d\beta} > 0$ in the right side of Eq. 7, and $\mu(a)$ needs to be a real valued function as well. Thus, depending on $k(a)$, Eq. 7, might have a solution, multiple solutions, or no solutions. By writing Eq. 7 in the following form and taking the derivative of this function, the resulting expressions are obtained:

$$\begin{aligned} F(\epsilon) &= 1 - \int_0^W k(\alpha)\mathrm{e}^{-\epsilon\alpha - \int_0^\alpha \mu(\beta)d\beta}d\alpha \\ \frac{dF(\epsilon)}{d\epsilon} &= \int_0^W \alpha k(\alpha)\mathrm{e}^{\epsilon\alpha - \int_0^\alpha \mu(\beta)d\beta}d\alpha \end{aligned} \tag{8}$$

Thus, if $F(\epsilon) = 0$, Eq. 7 holds. Considering that $k(a)$ is a real-valued function, some conclusions can be taken on the assumptions of $k(a)$:

1. $k(a) > 0, \forall\ 0 \leq a \leq W$, then $\int_0^W k(\alpha) \mathrm{e}^{-\epsilon\alpha - \int_0^\alpha \mu(\beta)d\beta} > 0$ and $F(\epsilon)$ might have a root. As $\dfrac{dF(\epsilon)}{d\epsilon} > 0$, $F(\epsilon)$ is increasing $\forall\, \epsilon \in \Re$, thus, if the root exists, it is unique;
2. $k(a) < 0, \forall\ 0 \leq a \leq W$, then $\int_0^W k(\alpha) \mathrm{e}^{-\epsilon\alpha - \int_0^\alpha \mu(\beta)d\beta} < 0$ and $F(\epsilon) \geq 1$, $\forall\, \epsilon \in \Re$ and there is no root of $F(\epsilon)$;
3. $k(a) = 0, \forall\ 0 \leq a \leq W$, then $\int_0^W k(\alpha) \mathrm{e}^{-\epsilon\alpha - \int_0^\alpha \mu(\beta)d\beta} = 0$ and $F(\epsilon) = 1\ \forall\, \epsilon \in \Re$. Thus, the root does not exist.
4. If $k(a)$ has positive and negative values, then $F(\epsilon)$ might have multiple roots;

Unfortunately, considering that $k(a)$ might have negative values does not have a physical meaning, as it would consider that some part of the population affects the birth rate negatively. Thus, $k(a) \geq 0, \forall\ 0 \leq a \leq W$ is considered in this contribution. If the root of Eq. 8 is found, $x(0)$ can be found by substituting the solution back in Eq. 8, which leads to:

$$x(0) = \frac{\epsilon - u_{SS}}{\int_0^W p(\alpha) \mathrm{e}^{-\epsilon\alpha - \int_0^\alpha \mu(\beta)d\beta} d\alpha} \tag{9}$$

and the steady-state profile defined in Eq. 6 is completely defined. Next, the linearization of Eq. 1 is considered using the possible steady-states defined in this section. Then, the stability of the linearized system around the steady states is analyzed.

Parameter Continuation

To assess how variations of the parameters affect the system behavior, a pseudo arclength continuation method is used to estimate changes in the steady-states and, consequently, the system's stability and eigenvalues distribution. Figure 2 illustrates how the method provides an initial guess for a general system's states (x_1 and x_2) given a change in the parameter. In this continuation method, the states and parameter are parameterized with respect to the arclength, and its tangent is used as an initial guess for the steady-states. Thus, if a fixed step of the arclength is considered, and using an approximation for the tangent, a new initial guess of the solution is obtained.

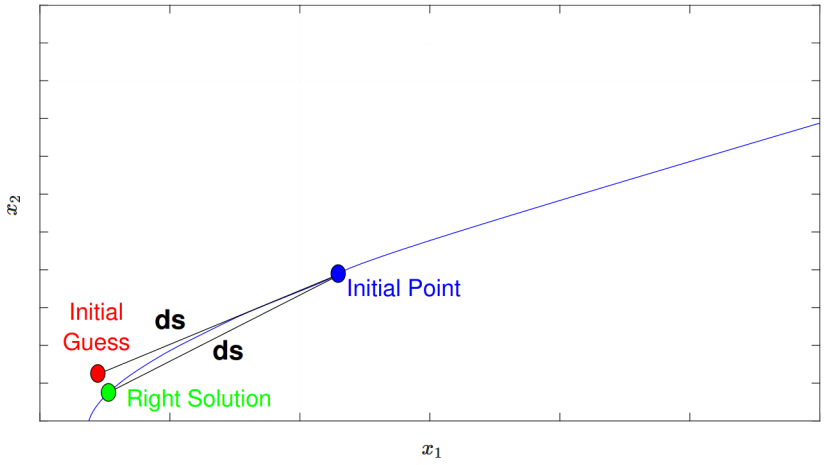

Figure 2: Representation of the Pseudo arclength method.

First, as shown in Eq. 10, a system of equations is solved to find the value of the tangents of the variable of interest (in this case, x) and the chosen parameter (β) with respect to the arclength (s) in a given iteration (k):

$$\begin{cases} J_k \left(\frac{dx}{ds}\right)_k + f_{\beta,k} \left(\frac{d\beta}{ds}\right)_k = 0 \\ \left(\frac{dx}{ds}\right)_k^T \left(\frac{dx}{ds}\right)_k + \left(\frac{d\beta}{ds}\right)_k^2 = 1 \end{cases} \tag{10}$$

where J_k is the Jacobian matrix (derivatives of the functions in respect to the states) in the step k and $f_{\beta,k}$ is a vector with the derivatives of the equations to the chosen parameter. Eq. 11 shows the first-order approximation used to calculate the initial guess for the next step of the parameter continuation analysis.

$$\begin{aligned} \left(\frac{dx}{ds}\right)_k &\approx \frac{x_{k+1} - x_k}{\Delta s} \rightarrow x_{k+1} = x_k + \left(\frac{dx}{ds}\right)_k \Delta s \\ \left(\frac{d\beta}{ds}\right)_k &\approx \frac{\beta_{k+1} - \beta_k}{\Delta s} \rightarrow \beta_{k+1} = \beta_k + \left(\frac{d\beta}{ds}\right)_k \Delta s \end{aligned} \tag{11}$$

where Δs is the arclength variation used and is a value that must be chosen. Finally, the new initial guesses for the variables of interest (x_{k+1}) and the system's parameter (β_{k+1}) are used in the system of equations that needs to be solved. If the value of Δs is appropriate, the values found for x_{k+1} and β_{k+1} are good guesses. Furthermore, one extra equation must be solved simultaneously with the system of equations to guarantee that the solution in the next step does not overstep the chosen variation of the arclength. These conditions are represented in Eq. 12.

$$\begin{cases} f(x_{k+1}, \beta_{k+1}) = 0 \\ (x_{k+1} - x_k) \left(\frac{dx}{ds}\right)_k + (\beta_{k+1} - \beta_k) \left(\frac{d\beta}{ds}\right)_k = \Delta s \end{cases} \tag{12}$$

For the chemostat reactor, the non-linear Eq. 7, related to the system steady-states, and the characteristic equation (Eq. 17), shown in the next section, make up the system of non-linear equations that need to be solved. The continuation method is used to investigate how the system's parameters influence the non-linear behavior and the system's steady state, considering a variation in different sets of parameters. The results for the variations in each of the system's parameters are shown in the results section.

Linearization

Defining $\bar{x}(t,a) = x(t,a) - x_{SS}(a)$, $\bar{u}(t) = u(t) - u_{SS}$ and $\bar{y} = y(t) - y_{SS}$, as the deviation variables from the states, the input and the output, respectively, to their steady-states found in the previous section, it is possible to write the linearized version of the system given in Eq. 1 as:

$$\begin{gathered} \frac{\partial \bar{x}}{\partial t} = -\frac{\partial \bar{x}}{\partial a} + \gamma(a)\bar{x} - x_{SS}(a)\int_0^W p(\alpha)\bar{x}(t,\alpha)d\alpha - x_{SS}(a)\bar{u}(t) \\ \bar{x}(t,0) = \int_0^W k(\alpha)\bar{x}(t,\alpha)d\alpha \\ \bar{y}(t) = \int_0^W \bar{x}(t,\alpha)d\alpha \end{gathered} \tag{13}$$

with:

$$\gamma(a) = -\left[\mu(a) + u_{SS} + \int_0^W p(\alpha)x_{SS}(\alpha)d\alpha\right] = -\left[\mu(a) + \epsilon\right] \tag{14}$$

and x_{SS} was defined in the previous section for a given value of u_{SS} and a set of parameters. For simplicity and ease of notation, all the following equations will use x, u, and y for the deviation variables instead of $\bar{x}$, $\bar{u}$ and $\bar{y}$. This linear system can be represented as an abstract state-space representation $[A, B, C, D]$ [22] given as:

$$\begin{cases} \dot{x}(t) = Ax(t) + Bu(t) \\ y(t) = Cx(t) + Du(t) \end{cases} \tag{15}$$

with:

$$\begin{gathered} A(\cdot) = -\frac{\partial(\cdot)}{\partial a} + \gamma(a)(\cdot) - x_{SS}(a)\int_0^W p(\alpha)(\cdot)d\alpha;\ B = -x_{SS}(a) \\ C(\cdot) = \int_0^W (\cdot)d\alpha;\ D = 0 \end{gathered} \tag{16}$$

where it is possible to see that $A \in$ is a linear integro-differential operator, $B \in$ is the in-domain input operator and $C \in$ is an integral output operator. The domain of the A operator can be defined as $D(A)\Big\{x \in X := L_2(0,W)\Big|x(a=0) = \int_0^W k(a)x(a)da\Big\}$.

Stability Analysis

For the linear operator A defined in Eq. 16, for a given set of parameter and a steady-state of the system found in the previous section, the eigenvalue problem $A\phi = \lambda\phi$, where ϕ are the eigenfunctions and λ are

the eigenvalues, yields the following characteristic equation for the system:

$$1 - \int_0^W k(a)f(a)da = 0 \tag{17}$$

with:

$$\begin{aligned} E(a) &= \mathrm{e}^{\int_0^W [\gamma(\alpha)-\lambda]d\alpha} \\ f(a) &= E(a) - E(a)\frac{I_p^W[E(a)]}{1 + I_p^W\{E(a)I_{\frac{1}{E}}^W[x_{SS}(\alpha)]\}} I_{\frac{1}{E}}^W[x_{SS}(\alpha)] \end{aligned} \tag{18}$$

where the integral operator $I_f^c(\cdot)$ is defined as $I_f^c(\cdot) = \int_0^c f(\alpha)(\cdot)d\alpha$. As the characteristic equation is non-linear, it is solved numerically in this contribution. The derivation of this equation can be found in Appendix A.

$$\phi(a) = c\left[-\frac{E(a)I_k^W\left\{E(a)I_{\frac{1}{E}}^W[x_{SS}(\alpha)]\right\}}{1 - I_k^W[E(a)]} - I_E^W(x_{SS}(\alpha))\right] \tag{19}$$

Bi-orthonormal Basis

The space $\mathcal{X}$ is equipped with the inner product $< x_1, x_2 >_{\mathcal{X}}$:

$$< x_1, x_2 >_{\mathcal{X}} = \int_0^W x_1(a)[\bar{x}_2(a)]da \tag{20}$$

where, $x_1, x_2 \in \mathcal{X}$, $\bar{x}_2$ is the complex conjugate of x_2. Using this definition of inner product, it is possible to find the adjoint operator of A, as shown in Appendix B:

$$\begin{aligned} A^*x = \frac{\partial x}{\partial a} + \gamma(a)x - p(a)\int_0^W x_{SS}(\alpha)x(\alpha)d\alpha + k(a)x(0), x(A) = 0; \\ B^*(\cdot) = \int_0^W [-x_{SS}(a)(\cdot)]da; C^* = 1;\ D^* = 0 \end{aligned} \tag{21}$$

And solving the eigenvalue problem for the adjoint operator ($A^*\psi = \lambda\psi$) leads to the adjoint eigenfunctions (ψ):

$$\psi(a) = c^*E^*(a)\left[1 - I_{\frac{1}{E}}^W[k(\alpha)] + I_{\frac{1}{E}}^W[p(\alpha)]\frac{I_{x_{SS}}^W\left[E^*(a)\left\{1 - I_{\frac{1}{E}}^W[k(\alpha)]\right\}\right]}{1 - I_{x_{SS}}^W\left[E^*(a)I_{\frac{1}{E}}^W[p(\alpha)]\right]}\right] \tag{22}$$

with:

$$E^*(a) = \mathrm{e}^{\int_0^W [\lambda-\gamma(\alpha)]d\alpha} \tag{23}$$

c^* can be set together with c from Eq. 19, such that the inner-product $< \phi_i, \bar{\psi}_i >= 1$.

Resolvent Operator

The resolvent operator, later used in the discrete representation of the system, is given as:

$$(sI - A)^{-1}x_0 = \frac{f(a)}{1 - \int_0^W k(a)f(a)da}\int_0^W k(\alpha)\Omega x_0(\alpha)d\alpha + \Omega x_0(a) \tag{24}$$

where $f(a)$ was defined in Eq. 18 and the operator $\Omega(\cdot)$ is:

$$\Omega x_0(a) = -\frac{w x_0}{1 + w x_{SS}} \int_0^W x_0(\alpha) \mathrm{e}^{\int_\alpha^W [\gamma(\beta) - s] d\beta} d\alpha + \int_0^W x_0(\alpha) \mathrm{e}^{\int_\alpha^W [\gamma(\beta) - s] d\beta} d\alpha \tag{25}$$

where w was defined in Eq. 18 as well. Notice that, as expected, the poles of the resolvent operator will be the same as the eigenvalues given by the characteristic equation shown in the previous section. The derivation of the resolvent operator is shown in Appendix C.

With the resolvent operator, it is also possible to define the other operators used in the discrete representation in the next section:

$$\begin{gathered}
(sI - A)^{-1} B = \frac{f(a)}{1 - \int_0^W k(a) f(a) da} \int_0^W k(a) \Omega B da + \Omega B = \\
- \frac{f(a)}{1 - \int_0^W k(a) f(a) da} \int_0^W k(a) \Omega x_{SS}(a) da - \Omega x_{SS}(a)
\end{gathered}$$

$$\begin{gathered}
C(sI - A)^{-1}(\cdot) = C \left(\frac{f(a)}{1 - \int_0^W k(a) f(a) da} \int_0^W k(a) \Omega x_0(a) da + \Omega x_0(a) \right) = \\
\frac{\int_0^W f(a) da}{1 - \int_0^W k(a) f(a) da} \int_0^W k(a) \Omega(\cdot) da + \int_0^W \Omega(\cdot) da
\end{gathered} \tag{26}$$

$$\begin{gathered}
C(sI - A)^{-1} B = \frac{\int_0^W f(a) da}{1 - \int_0^W k(a) f(a) da} \int_0^W k(a) \Omega B da + \Omega B = \\
- \frac{\int_0^W f(a) da}{1 - \int_0^W k(a) f(a) da} \int_0^W k(a) \Omega x_{SS}(a) da - \int_0^W \Omega x_{SS}(a) da
\end{gathered}$$

Thus, it is possible to see that $(sI - A)^{-1} B$ is a spatial function on the domain and does not change for a given x_{SS}, $C(sI - A)^{-1}(\cdot)$ operates on a spatial function and gives a scalar number. Thus, $C(sI - A)^{-1} B$ will be just a scalar number for a given x_{SS}.

Discrete Representation

Given the system defined in Eq. 15, applying the Crank-Nicolson midpoint integration rule and considering piecewise constant input within the discretization interval (known as the Cayley-Tustin time discretization transformation), a structure-preserving discrete representation of the system is obtained. The discrete system is represented by:

$$\begin{aligned}
x_{k+1} &= A_d x_k + B_d u_k \\
y_k &= C_d x_k + D_d u_k
\end{aligned} \tag{27}$$

where A_d, B_d, C_d and D_d are the discrete-time system operators and are given by:

$$\begin{bmatrix} A_d & B_d \\ C_d & D_d \end{bmatrix} = \begin{bmatrix} -I + 2\delta \left(\delta I - A\right)^{-1} & \sqrt{2\delta} \left(\delta I - A\right)^{-1} B \\ \sqrt{2\delta} C \left(\delta I - A\right)^{-1} & C \left(\delta I - A\right)^{-1} B \end{bmatrix} \tag{28}$$

and $\delta = 2/\Delta t$, $\left(\delta I - A\right)^{-1} = R(\delta, A)$ is the resolvent operator of A and these operators can be found in Eqs. 24 and 26.

Discrete System Stabilization

First, it is assumed that full state feedback is available, such that the following control law is considered for the system's stabilization:

$$\begin{aligned} x_{k+1} &= A_d x_k + B_d u_k \\ u_k &= K_d x_k \end{aligned} \tag{29}$$

where A_d, B_d have been defined previously, and K_d is the full state feedback controller gain in the discrete-time setting. The controller takes the values of the states x_{k-1} and calculates the desired u_k that stabilizes the closed-loop system. To this end, the proper controller gain (K_d) needs to be found for the closed-loop dynamics ($A_d + B_d K_d$) to be stable and $x_k \to 0$ as $k \to \infty$. As shown in Appendix D, the following discrete Ricatti equation can be solved to find the required controller gain:

$$\left\langle x, A_d^* \bar{Q}_C A_d x \right\rangle - \left\langle x, \bar{Q}_C x \right\rangle - \left\langle x, (A_d^* \bar{Q}_C B_d)(R + B_d^* \bar{Q}_C B_d)^{-1} (B_d^* \bar{Q}_C A_d) x \right\rangle = - \left\langle x, Q_C x \right\rangle \tag{30}$$

and the controller gain will then be given as $K_d(\cdot) = -(R + B_d^* \bar{Q}_C B_d)^{-1}(B_d^* \bar{Q}_C A_d)(\cdot)$. Solving this equation with the inner product is the same as solving the following equation:

$$A_d^* \bar{Q}_C A_d - \bar{Q}_C - (A_d^* \bar{Q}_C B_d)(R + B_d^* \bar{Q}_C B_d)^{-1}(B_d^* \bar{Q}_C A_d) = -Q_C \tag{31}$$

which is the discrete Ricatti equation generally used for finite (lumped) systems. Solving any of these Ricatti equations is analog to solving the following discrete Lyapunov equation:

$$< \bar{Q}_C (A_d + B_d K_d) x, (A_d + B_d K_d) x > - < \bar{Q}_C x, x > = - < x, (Q_C + K_d^* R K_d) x > \tag{32}$$

Thus, if $\bar{Q}_C$ and Q are positive definite operators, the closed-loop dynamics $A_d - B_d K_d$ is stable. By using the bi-orthogonal basis of A and its projections, the Ricatti equation can be written as:

$$\begin{gathered} \lambda_N^D q_{N,M}^c \lambda_M^D - q_{N,M}^c - (\lambda_N^D \textstyle\sum_j q_{N,j}^c b_j)^T (R + \sum_i \sum_j b_i^* q_{i,j}^c b_j)^{-1} \overline{\lambda}_M^D (\sum_j q_{M,j}^c b_j) = \\ -(\psi_N)^T Q_C \overline{\psi_M} \end{gathered} \tag{33}$$

where $b_j = B_d^* \psi$, ψ_i are the adjoint system's eigenfunctions, and λ_i^D are the eigenvalues in the discrete-time setting, defined previously.

Thus, this system of non-linear equations can be solved to find each $q_{N,M}^c$ and, consequently, $K_d(\cdot)$ can be properly defined:

$$\begin{gathered} \bar{Q}_C(\cdot) = \textstyle\sum_i^N \sum_j^N q_{i,j}^c < (\cdot), \overline{\psi}_i > \overline{\psi}_j; \\ K_d(\cdot) = (R + B_d^* \bar{Q}_C B_d)^{-1}(B_d^* \bar{Q}_C A_d)(\cdot) = (R + \textstyle\sum_i \sum_j b_i^* q_{i,j}^c b_j)^{-1} \sum_i^N \sum_j^N q_{i,j}^c < (\cdot), \bar{\lambda}_i^D \bar{\psi}_i > b_j \end{gathered} \tag{34}$$

It is important to notice that, for an infinite-dimensional system $N \to \infty$, this type of system has an infinite number of eigenvalues, as shown in the previous sections. Thus, we consider the controller gain approximation using a finite number of eigenvalues. As the system considered is linear, a direct relationship between the discrete and continuous eigenvalues can be obtained. For the Cayley-Tustin time discretization used, this relation is given by $\lambda_i^D = -1 + \frac{2\delta}{\delta - \lambda_i}$, where λ_i^D and λ_i are the eigenvalues in the discrete and continuous time setting, respectively. Furthermore, for a linear system, the eigenfunctions associated with the spatial characteristics are invariant (the same as in the continuous time setting).

Discrete System Observer

The closed-loop stabilization developed in the previous section considers full-state feedback. Unfortunately, that is entirely unfeasible for infinite dimensional systems, as it would require at least a large number of measurements. This type of sampling becomes impossible for the chemostat reactor, requiring the separation of specific ages of the population inside the reactor. Thus, a Luenberger observer is considered for state reconstruction based only on the system output (the measured mass of a sample in a given time). The Luenberger observer in the discrete-time setting is defined as follows:

$$\begin{aligned} \hat{y}_k &= C_d \hat{x}_k + D_d u_k \\ \hat{x}_{k+1} &= A_d \hat{x}_k + B_d u_k + L_{o,d}\left[y_k - \hat{y}_k\right] \end{aligned} \tag{35}$$

where $A_d, B_d, C_{m,d} D_d$ have been defined previously and $L_{o,d}$ is the observer gain in the discrete time setting. The observer takes the current values of $y_{m,k}$ and u_k as input and gives the current state estimation $\hat{x}_k$, which is used in the controller to calculate the input to the system in the next time step. Thus, the proper observer gain ($L_{o,d}$) needs to be found, such that the observer error dynamics, defined as $\hat{e}_k = x_k - \hat{x}_k$, is stable and $\hat{x}_k \to x_k$ as $k \to \infty$. As shown in Appendix E, the following discrete Ricatti equation can be solved to find the appropriate observer gain:

$$\begin{aligned} < \bar{Q}_O A_d^* x, A_d^* x > - < \bar{Q}_O x, x > - < (I + C_d \bar{Q}_O C_d^*)^{-1} C_d \bar{Q}_O A_d^* x, C_d \bar{Q}_O A_d^* x >= \\ - < Q_O C_d x, C_d x > \end{aligned} \tag{36}$$

where the observer gain will then be given as $L_{o,d} = A_d^* \bar{Q}_O C_{m,d}^* (I + C_{m,d} \bar{Q}_O C_{m,d}^*)^{-1}$. Similarly to the controller design, solving this equation using the inner product is the same as solving the following equation:

$$A_d \bar{Q}_O A_d^* - \bar{Q}_O - A_d \bar{Q}_O C_d^* (I + C_d \bar{Q}_O C_d^*)^{-1} C_d \bar{Q}_O A_d^* = -C_d^* Q_O C_d \tag{37}$$

which is the discrete Ricatti equation generally used for finite (lumped) systems in the observer design. These equations are related to the following Lyapunov equation:

$$< \bar{Q}_O (A_d - L_{o,d} C_d)^* x, (A_d - L_{o,d} C_d)^* x > - < \bar{Q}_O x, x >= - < x, (C_d^* Q_O C_d + L_{o,d} L_{o,d}^*) x > \tag{38}$$

Thus, if $\bar{Q}_O$ and Q_O are positive definite operators, the observer dynamics $A_d - L_{o,d} C_{m,d}$ is stable, and the observer states converge to the system states. Once again, the Ricatti equation can be rewritten by using the bi-orthogonal basis of A:

$$\begin{aligned} \lambda_M^D \lambda_N^D q_{N,M}^o - q_{N,M}^o - (\lambda_N^D \textstyle\sum_i c_i q_{N,i}^o)^T (I + \sum_i \sum_j c_i^* q_{i,j}^o c_j)^{-1} \overline{(\lambda_M^D \sum_i c_i q_{M,i}^o)} = \\ -(C_d \psi_N)^T Q_O \overline{(C_d \psi_M)} \end{aligned} \tag{39}$$

where $c_i = C_{m,d} \phi_i$. Thus, this system of non-linear equations can be solved to find each $q_{N,M}^o$ and, consequently, $\bar{Q}_O(\cdot)$, such that the observer gain is given by $L_{o,d} = A_d \bar{Q}_O C_{m,d}^*$:

$$\begin{aligned} \bar{Q}_O(\cdot) &= \textstyle\sum_i^N \sum_j^N q_{i,j}^o < \phi_i, (\cdot) > \phi_j; \\ L_{o,d}(\zeta) = A_d \bar{Q}_O C_d^* &= \textstyle\sum_i^N \sum_j^N q_{i,j}^o \lambda_j^D \phi_j(\zeta) < C_d \phi_i, 1 > \end{aligned} \tag{40}$$

Similarly to the controller gain, an approximation of the observer gain is considered by using a finite number of eigenvalues.

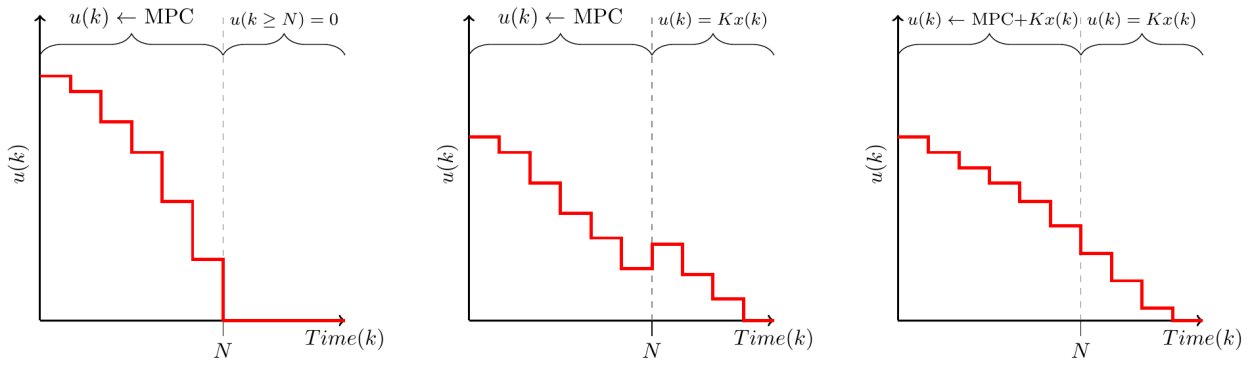

a) MPC used in [20] b) "Switching" Dual-mode used in [21] c) Dual-mode used in this contribution

Figure 3: Different types of MPC strategies found in the literature;

In this contribution, the MPC design developed in [20] is extended to consider the two types of control strategies used, similarly to [21]. Figure 3 show the difference in the control strategy between this contribution and previous contributions. In [20], the MPC was designed to calculate all the actions within the control horizon, and stability constraints were imposed at the end of the horizon such that no more actions would be necessary for stabilization (i.e., the input - $u(k)$ - was 0 for any $k \geq N$). Thus, if the optimization problem in the control horizon is feasible, any unstable modes would be canceled, and the system states would reach the origin in the open-loop dynamic. In [21], a "switching" dual-mode MPC was used, where the MPC actions were calculated in the control horizon, and a (state or output) feedback control law was used after the control horizon. If this control law is related to an optimal cost with different weights as the MPC, there will be a switching in the control strategy.

Similarly to [21], in this contribution, a dual-mode MPC is also used, but the controller takes into account the feedback control law inside the control horizon as well. Thus, the input can be written as $u(k) = Kx(k) + v(k)$, where K is the feedback gain (where obtained as the solution of an LQR problem) and $v(k)$ are the control actions calculated in the MPC. The minimization of the following objective function provides the necessary input at each sampling time (k) on an infinite horizon:

$$\begin{aligned} \min_{v} \sum_{l=0}^{\infty} & < x(k+l|k), Q_{MPC} x(k+l|k) > + < u(k+l|k), R_{MPC} u(k+l+1|k) > \\ \text{s.t.} \quad & x(k+l+1|k) = A_d x(k+l|k) + B_d u(k+l|k), \\ & y(k+l|k) = C_d x(k+l|k) + D_d u(k+l|k), \\ & u(k+l|k) = K_d x(k+l|k) + v(k+l|k), \\ & u^{\min} \leqslant u(k+l|k) \leqslant u^{\max}, \\ & y^{\min} \leqslant y(k+l|k) \leqslant y^{\max} \end{aligned} \tag{41}$$

where R_{MPC} is the input cost; Q_{MPC} represents the states cost and is a positive semidefinite operator; $(k+l|k)$ are the predictions of the model at the current step; $u^{\min}$ and $u^{\max}$ are, respectively, the minimum

and maximum constraints on the input; $y^{\min}$ and $y^{\max}$ are the minimum and maximum constraints in the desired output. As the feedback gain guarantees the stability of the closed-loop system, the MPC only takes action (i.e., $v(k) \neq 0$) in two cases: the constraints are not satisfied within the control horizon, thus the MPC changes the feedback action to guarantee it; or, the feedback gain used is not the solution of an LQR problem with the same Q_{MPC} and R_{MPC}, and the state feedback actions are not optimal to the same objective function. For simplicity, in this contribution, only the first case is considered, such that $Q_{LQR} = Q_{MPC} = Q_C$ and $R_{LQR} = R_{MPC} = R$. If the MPC acts on a given control horizon, N, and only the state feedback controller is used after (i.e., $v(k \geq N+1|k) = 0$), the objective function given by Eq. 41 can be rewritten as:

$$\begin{aligned}
&J = \textstyle\sum_{l=0}^{N-1} \{< x(k+l|k), Q_C x(k+l|k) > + < u(k+l|k), Ru(k+l|k) >\} + \\
&\textstyle\sum_{l=N}^{\infty} \{< x(k+l|k), Q_C x(k+l|k) > + < u(k+l+1|k), Ru(k+l|k) >\} = \\
&\textstyle\sum_{l=0}^{N-1} \{< x(k+l|k), Q_C x(k+l|k) > + < \left[K_d x(k+l|k) + v(k+l|k)\right], R\left[K_d x(k+l|k) + v(k+l|k)\right] >\} + \\
&\textstyle\sum_{l=N}^{\infty} \{< x(k+l|k), Q_C x(k+l|k) > + < K_d x(k+l|k), RK_d x(k+l|k) >\} = \\
&\textstyle\sum_{l=0}^{N-1} \{< x(k+l|k), \left[K_d^* R K_d + Q_C\right] x(k+l|k) > + < v(k+l|k), Rv(k+l|k) > + \\
&< v(k+l|k), RK_d x(k+l|k) > + < K_d x(k+l|k), Rv(k+l|k) > \} \\
&\textstyle\sum_{l=N}^{\infty} \{< x(k+l|k), \left[K_d^* R K_d + Q_C\right] x(k+l|k) >\} = \\
&\textstyle\sum_{l=0}^{N-1} \{< x(k+l|k), \left[K_d^* R K_d + Q_C\right] x(k+l|k) > + < v(k+l|k), Rv(k+l|k) > + \\
&< v(k+l|k), RK_d x(k+l|k) > + < K_d x(k+l|k), Rv(k+l|k) > \} \\
&< x(k+l+N|k), \bar{Q}_C x(k+l+N|k) >
\end{aligned} \tag{42}$$

where $u(k+l|k) = K_d x(k+l|k) + v(k+l|k)$ was used to write the equation as a function of $v(k)$ instead of $u(k)$, and, as the last step, the fact that the solution of the Ricatti equation shown in Eq. 34 is the solution of the corresponding Lyapunov equation shown in Eq. 32 was considered. Thus, the last term represents the terminal cost of the closed-loop system under the state feedback control law only after the control horizon. The optimization problem then becomes:

$$\begin{aligned}
&\min_{v} \sum_{l=0}^{N-1} \{< x(k+l|k), \left[K_d^* R K_d + Q_C\right] x(k+l|k) > + < v(k+l|k), Rv(k+l|k) > + \\
&< v(k+l|k), RK_d x(k+l|k) > + < K_d x(k+l|k), Rv(k+l|k) > \} + < x(k+l+N|k), \bar{Q}_C x(k+l+N|k) > \\
&\text{s.t.} \quad x(k+l+1|k) = \bar{A}_d x(k+l|k) + B_d v(k+l|k), \\
&\qquad y(k+l|k) = (C_d + D_d K_d) x(k+l|k) + D_d v(k+l|k), \\
&\qquad u^{\min} \leqslant K_d x(k+l|k) + v(k+l|k) \leqslant u^{\max}, \\
&\qquad y^{\min} \leqslant y(k+l|k) \leqslant y^{\max}
\end{aligned} \tag{43}$$

where $\bar{A}_d = A_d + B_d K_d$. Finally, Eq. 43 can be rewritten in a quadratic optimization form:

$$\begin{aligned} \min_{V} \quad & J = 2V^T G[x(\zeta, k|k)] \\ & + V^T H V + < x(k|k), \bar{Q}_C x(k|k) > \\ \text{s.t.:} \quad & \\ & U^{\min} \leqslant MV + N[x(\zeta, k|k)] \leqslant U^{\max} \\ & Y^{\min} \leqslant SV + T[x(\zeta, k|k)] \leqslant Y^{\max} \end{aligned} \tag{44}$$

The elements of each operator and matrices defined on Eq. 44 are given by:

$$h_{i,j} = \begin{cases} \left[B_d, \bar{Q}_C B_d\right] + R, \text{ if } i = j \\ \left[B_d, \bar{Q}_C (\bar{A}_d)^{(i-j)} B_d\right] + \left[R, K_{F,D} (\bar{A}_d)^{(i-j)} B_d\right], \text{ if } i > j \\ \left[(\bar{A}_d)^{(j-i)} B_d, \bar{Q}_C B_d\right] + \left[K_{F,D} (\bar{A}_d)^{(i-j)} B_d, R\right], \text{ if } i < j \end{cases}$$

$$G[\cdot] = \begin{bmatrix} [B_d, \bar{Q}_C \bar{A}_d(\cdot)] + [R, K_d I(\cdot)] \\ [B_d, \bar{Q}_C (\bar{A}_d)^2(\cdot)] + [R, K_d \bar{A}_d(\cdot)] \\ \vdots \\ [B_d, \bar{Q}_C (\bar{A}_d)^N(\cdot)] + [R, K_d \bar{A}_d^{N-1}(\cdot)] \end{bmatrix}, \; T[\cdot] = \begin{bmatrix} C_d(\cdot) \\ C_d(\bar{A}_d)(\cdot) \\ \vdots \\ C_d(\bar{A}_d)^{N-1}(\cdot) \end{bmatrix}$$

$$N[\cdot] = \begin{bmatrix} K_d(\cdot) \\ K_d \bar{A}_d(\cdot) \\ \vdots \\ K_d \bar{A}_d^{N-1}(\cdot) \end{bmatrix}$$

$$M = \begin{bmatrix} I & 0 & \dots & 0 \\ K_d B_d & I & \dots & 0 \\ \vdots & \vdots & \ddots & \vdots \\ K_d (\bar{A}_d)^{N-2} B_d & K_d (\bar{A}_d)^{N-3} B_d & \dots & I \end{bmatrix}$$

$$V = \begin{bmatrix} v(k+1|k) & v(k+2|k) & \dots & v(k+N|k) \end{bmatrix}^T$$

$$S = \begin{bmatrix} D_d & 0 & \dots & 0 \\ C_d B_d & D_d & \dots & 0 \\ \vdots & \vdots & \ddots & \vdots \\ C_d (A_d)^{N-2} B_d & C_d (A_d)^{N-3} B_d & \dots & D_d \end{bmatrix}$$

$$V = \begin{bmatrix} v(k+1|k) & v(k+2|k) & \dots & v(k+N|k) \end{bmatrix}^T$$

where the operation $[x, B_d]$ is defined as the inner product, but with v separated, such that $[x, B_d]v =< x, B_d v >$ or $v^T(k)[B_d, x] =< B_d v, x >$ as $v(k)$ is considered to be a real valued. Thus, this operation will not necessarily give a scalar number, as is expected from the inner product.

Results

This contribution's results are shown in this section. Table 1 shows the parameters and conditions used. The results consider this set of parameters, except the parameter continuation results. First, the non-zero steady-state is shown, and it is possible to conclude that the open-loop system is unstable by its eigenvalue distribution. The effect of the parameters on the stability and steady-state profile is shown after. Lastly, the simulation results for the dual-mode MPC are presented using the controller and observer design derived in the previous sections.

Parameter	u_{SS}	$\mu(a)$	$k(a)$	$p(a)$	μ_0
Value	0.2	$\mu_0 \mathrm{e}^{\mu_b a}$	$k_0 \mathrm{e}^{k_b a}$	$p_0 - p_b \sin\left(\frac{a\pi}{2} a\right)$	0.8
Parameter	μ_b	k_0	k_b	p_0	p_b
Value	1.5	0.5	0.5	0.2	1.2

Table 1: Functions and parameters used in the simulation;

For the mortality, birth, and self-competition rate functions shown in Table 1, the non-zero solution of the non-linear equations given by Eqs. 4 - 7 is shown in Figure 4. This is the steady state of interest and, as shown next, is an unstable steady state of the system. Thus, using the biorthonormal basis, the system can be stabilized in this operating condition using a full-state feedback law obtained by solving the Ricatti equation given by Eq. 30. This guarantees closed-loop stability. However, not the constraints satisfaction. Due to this fact, the Dual-mode MPC is used, changing the value of the input as necessary.

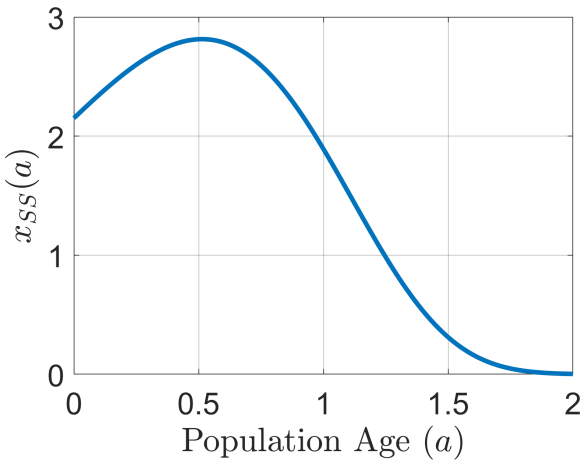

Figure 4: Population steady-state for the parameters given in Table 1;

Eigenvalue Distribution and Eigenfunctions

By numerically solving the system's characteristic equation given by Eq. 17, the eigenvalue distribution is shown in Figure 5. The open-loop system has one unstable real eigenvalue, and all others are complex conjugated pairs located at the left side of the complex plane. The figure also compares the eigenvalue distribution of the linearized operator given by Eq. 13, if an early-lumping approach is considered. This distribution is obtained using the finite-difference method to approximate the spatial derivative and the trapezoidal rule to approximate the integral operator. It is possible to notice that, even though the early-lumping approach can adequately capture the behavior of the unstable eigenvalue and the first three pairs of complex conjugate eigenvalues, the rest of the distribution is entirely off when compared to the solution of the system's characteristic equation. This distribution also depends on the number of spatial discretization points used. In Figure 5, 200 discretization points were used. If a few points are used, the proper mapping of the first three pairs of eigenvalues is not guaranteed.

Interestingly enough, the behavior of the distribution is also completely different. The solution of the characteristic equation predicts that the eigenvalues are distributed in an almost vertical stripe that crosses the complex plane, where all the eigenvalues have the same real part. On the other hand, the distribution given by the early-lumping approach shows that the eigenvalues are distributed in a circle, with the real components of the eigenvalues showing. This can lead to entirely different dynamic behavior. This is one of the reasons that the Cayley-Tustin time discretization is considered in this contribution, which can be applied as a late-lumping approach. Although this discretization scheme approximates the system dynamics, it adequately represents the original system's stability in the discrete-time setting (i.e., unstable modes in the continuous-time setting will be mapped to unstable modes in the discrete-time setting).

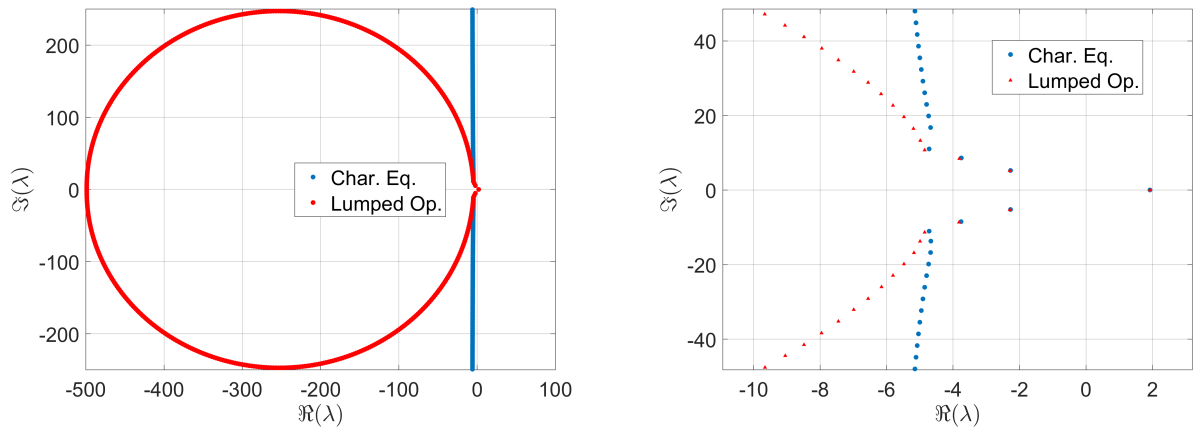

a) Eigenvalue Distribution

b) Close-in of the Eigenvalue Distribution

Figure 5: Eigenvalue distribution, comparison between the distribution obtained by the early-lumping approach and the solution of the characteristic equation;

The eigenfunctions of the system related to the first three eigenvalues (the unstable real one and the

first pair of complex eigenvalues) are shown in Figure 6. As expected, the eigenfunction related to the real eigenvalue is a real function. At the same time, the same happens to the eigenfunctions associated with the complex pair of eigenvalues (i.e., the complex eigenvalue leads to a complex eigenfunction). With the defined eigenvalues and eigenfunctions, the Ricatti equations shown in Eq. 34 and Eq. 40 can be solved, and the full-state feedback gain that stabilizes the discrete system and the observer gain that ensures the system states reconstruction can be obtained.

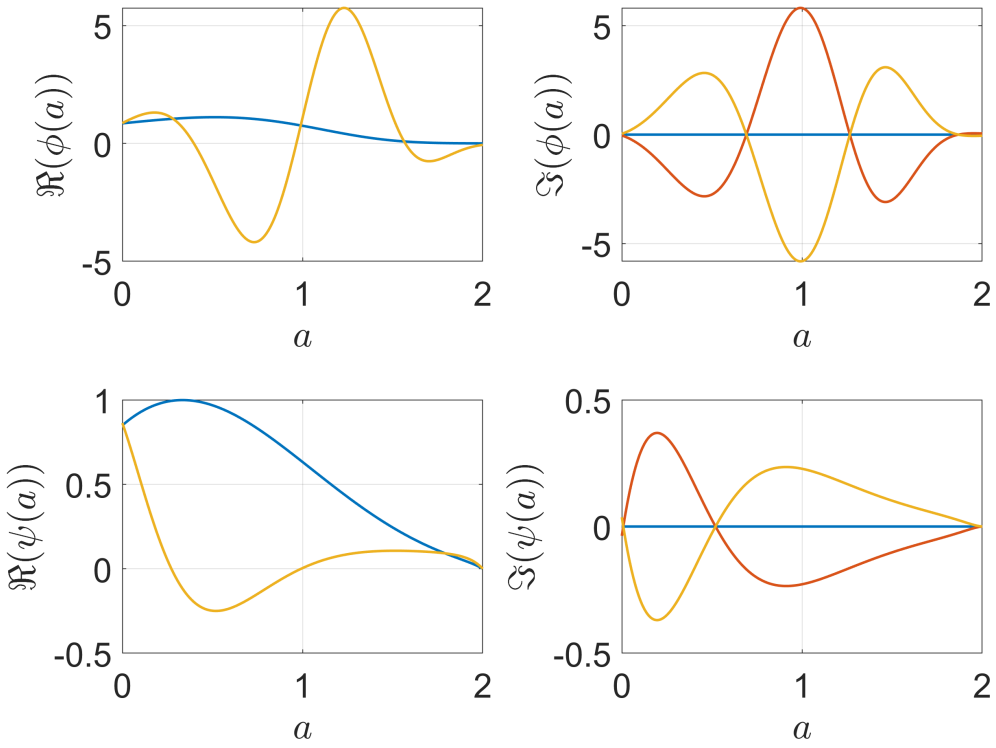

Figure 6: Eigenfunctions related to the first three eigenvalues given by the characteristic equation (Eq. 19): (Top-left) Real values of the eigenfunctions of A; (Top-right) Imaginary values of the eigenfunctions of A; (Bottom-left) Real values of the eigenfunctions of A^*; (Bottom-right) Imaginary values of the eigenfunctions of A^*;

Parameter Continuation

In this section, the results show the behavior of the system steady-states and eigenvalue distribution for changes in the parameters (and input, u_{SS}) using the continuation method shown in the previous sections. For all the results displaying the eigenvalue distribution, a red "$\times$" shows the final value of the range considered, while a red circle represents the initial value. Only the non-zero steady-state is analyzed in this section, as it generally is the operating condition of interest. Overall, each parameter affects the steady-state and the eigenvalue distribution differently. Thus, the analysis for each one is carried out separately.

The first parameter analyzed is k_0, related to the birth rate $k(a) = k_0 e^{k_b a}$. As shown in Figures 7 and 8, reducing this parameter decreases the overall birth rate of the population. Thus, a larger population is necessary to maintain the equilibrium between the death, birth, and self-competition rates. Thus, as

$k_0 \to 0$, $\exists a$ such that $x_{SS}(a) \to \infty$ and $y_{SS}(a) \to \infty$. If $k_0 \to \infty$, then the opposite happens, and the overall population and the system output (the total mass/concentration of the population) decrease. It is important to notice that, although the total population decreases as k_0 increases, the population at $a = 0$ increases to a point with k_0 and then decreases. The parameter affects the whole eigenvalue distribution, and as it increases, the distribution is shifted to the left side of the complex plane.

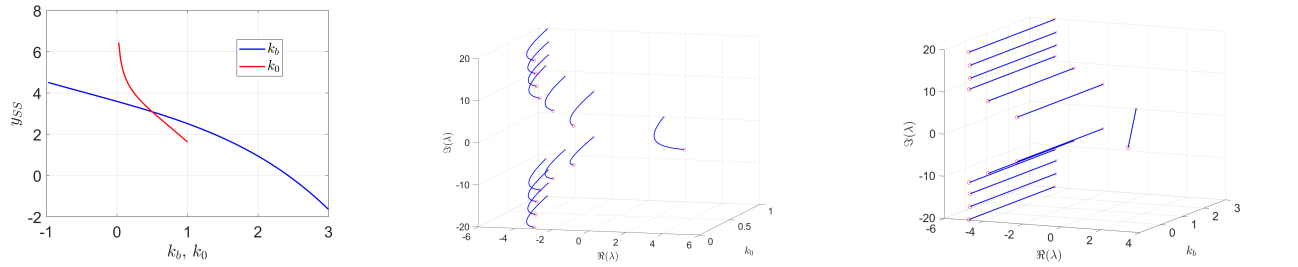

a) $y_{SS}(k_0)$ & $y_{SS}(k_b)$ b) Eigenvalues Distribution as a function of k_0 c) Eigenvalues Distribution as a function of k_b

Figure 7: Output and eigenvalues distribution for different values of k_0 and k_b;

Next, the effects of k_b are discussed and shown in Figures 7 and 8 as well. Similarly to k_0, as k_b decreases, the overall population and the system output increase. However, the steady-state is expected to have negative values for large values, which is not physically viable. Hence, unlike k_0, this parameter only affects the real eigenvalue, while the others remain unaffected.

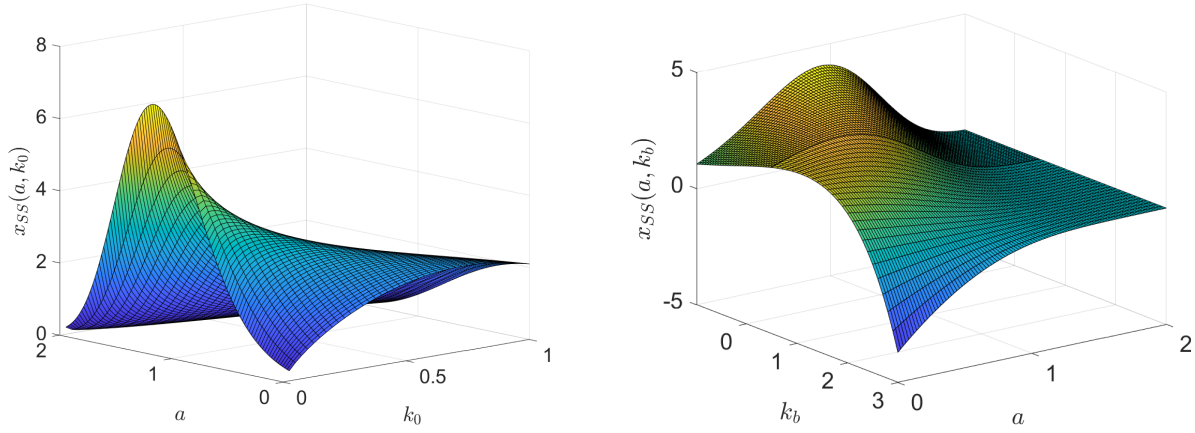

a) $x_{SS}(a, k_0)$ b) $x_{SS}(a, k_b)$

Figure 8: System steady-states for different values of k_0 and k_b;

The effects of μ_b are shown in Figures 9 and 10. As the parameter is related to the mortality rate by $\mu(a) = \mu_0 e^{\mu_b a}$, one expects an opposite behavior from what was analyzed for k_0 and k_b. As μ_b increases, the overall population at steady-state also increases. This is necessary to maintain the equilibrium between

the different rates affecting the system. When the opposite happens and $\mu_b \to 0$, the overall population and the system output decrease. The eigenvalue distribution is also completely affected by changes in this parameter, with the real unstable eigenvalue shifting further into the right side of the complex plane and the stable eigenvalues (with negative real parts) shifting further to the left.

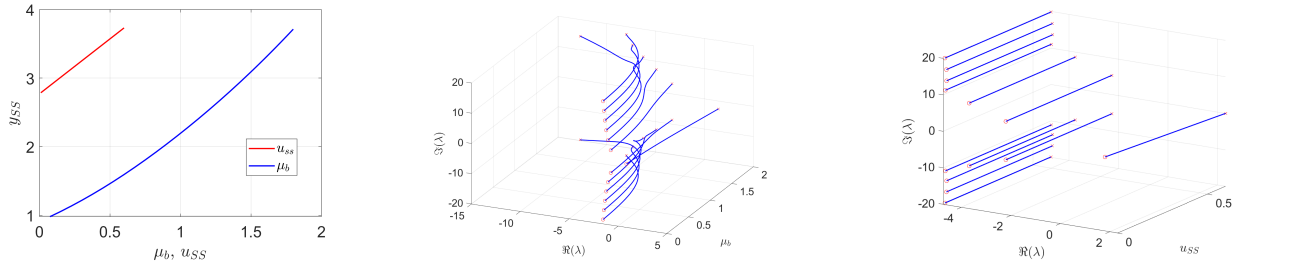

a) $y_{SS}(\mu_b)$ & $y_{SS}(u_{ss})$ b) Eigenvalues Distribution as a function of μ_b c) Eigenvalues Distribution as a function of u_{ss}

Figure 9: Output and eigenvalues distribution for different values of μ_b and u_{ss};

Lastly, the effects of the input u_{SS} in the system are analyzed. As the input is related to the dilution rate of the system, the higher the dilution rate is, the higher the increase in the steady-state population to counter the effects of the dilution. It is important to notice that the steady state is always unstable, and an increase in the input further shifts the unstable eigenvalue to the right side of the plan while the others remain unaffected.

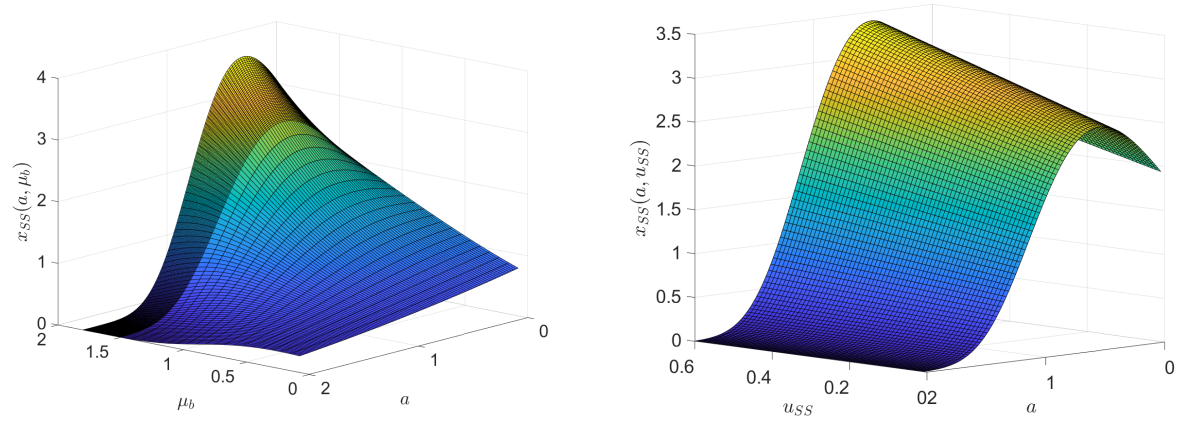

a) $x_{SS}(a, \mu_b)$ b) $x_{SS}(a, u_{ss})$

Figure 10: System steady-states for different values of μ_b and u_{ss};

Model Predictive Controller

In this section, the simulation results of the dual-mode MPC implementation in the system are shown. The unstable steady-state shown previously is considered as the target operating condition. The Ricatti

equation solved in Eq. 34 and the MPC use the same state and input costs (Q and R), which are shown in Table 2. The initial condition, in deviation from the steady-state profile, is chosen as $x(a, t = 0) = 0.2a^2 - 0.1427a - 0.2 + 0.65\sin(2\pi a)$, such that $x(a, 0) \in \mathcal{X}$. Four simulation results are shown below: unconstrained full-state feedback; unconstrained output feedback (observer-based); output feedback with input constraints; and output feedback with input and output constraints.

Parameter	u_{SS}	$\mu(a)$	$k(a)$	$p(a)$	μ_0
Value	0.2	$\mu_0 e^{\mu_b a}$	$k_0 e^{k_b a}$	$p_0 - p_b \sin\left(\frac{a\pi}{2} a\right)$	0.8
Parameter	μ_b	k_0	k_b	p_0	p_b
Value	1.5	0.5	0.5	0.2	1.2

Table 2: Control parameters used in the simulation;

As the same state and input costs are considered in the MPC and full-state feedback stabilization, it is expected that the optimal control sequence for the cost function to be the same as the ones given by the full-state feedback control law obtained with the solution of the Ricatti equation. Thus, $v(k)$, the control input calculated by the dual-mode MPC, is zero (i.e., $v(k) = 0, \forall\, k$). This is shown in Figure 11: the red line on the figure on the right represents $v(k)$ and is equal to zero for the whole simulation time. The blue line in the right figure shows the system norm for the simulation time, which is defined as $||x(a,k)|| = \sqrt{\int_0^W x^2(a,k)da}$. As expected from the full-state feedback stabilization, the system states and the norm decay with time, so the system states (the deviation from the system's actual states to the steady state) will reach the origin. The control input is represented by the black line in the right figure.

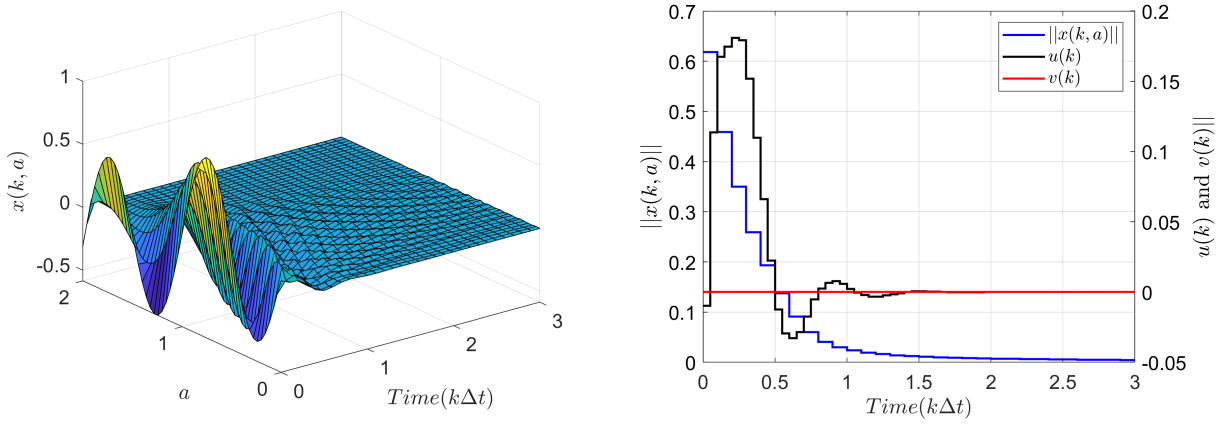

a) System states under full-state feedback

(Left axis) States norm;
(Right axis) Total input and MPC action;

Figure 11: System states and their norm under the control law of the Dual mode MPC;

As full-state feedback is not feasible for distributed systems, especially the chemostat reactor, the con-

troller's performance uses the observer-reconstructed states instead of the full-state. The results are shown in Figure 12. The initial condition for the observer was set as $\hat{x}(a,0) = 0$. For this reason, as the MPC is now using the observer states in the optimization problem, the first input of the control sequence is 0. After the first step, the observer states start to change, and the control input changes accordingly.

The observer error norm, defined as $||\hat{e}(a,k)|| = \sqrt{\int_0^W \hat{e}^2(a,k)da}$, with $\hat{e}(a,k) = x(a,k) - \hat{x}(a,k)$ is shown as the green line on the right figure. With the appropriate gain calculated by the Ricatti equation shown in Eq. 34, the observer states converge to the system states, and the observer error decreases, which is represented by its norm. The actions taken by the controller are higher when compared to the full-state feedback, as the controller does not have the correct states' values. As the observer states converge to the system states, the controller takes the appropriate actions, stabilizing the system. The difference in the control actions is slight but noticeable compared to Figure 11. As no constraints are imposed in the input or output of the system, and the same state and input costs are used for the full-state feedback control law, then the MPC does not need to shift the value of the full-state feedback and, again, $v(k) = 0$, $\forall k$.

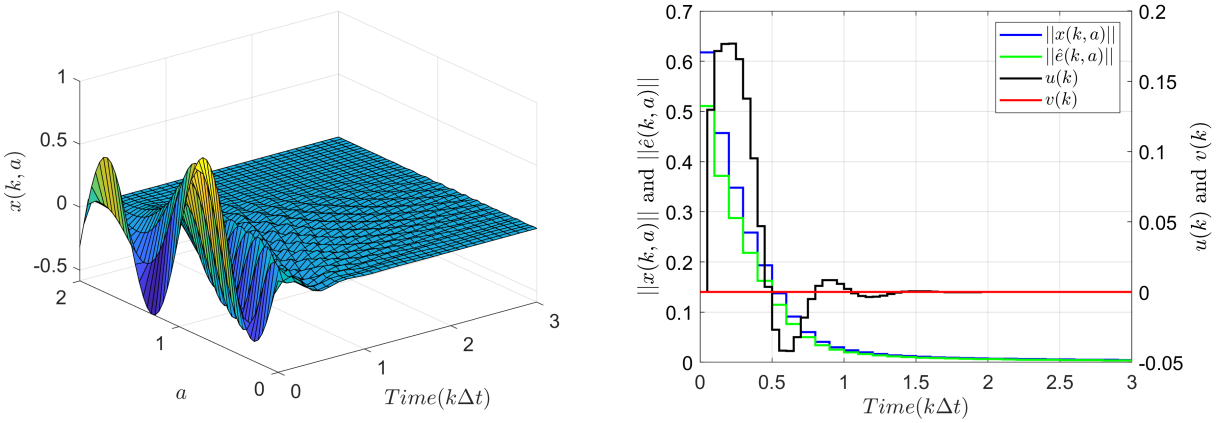

a) System states under output feedback

b) (Left axis) States norm;
(Right axis) Total input and MPC action;

Figure 12: System states, observer error and states norms under the control law of the Dual mode MPC without constraints;

Contrary to the previous cases, Figure 13 shows the controller and system responses when an input constraint is imposed. A maximum input of $u_{max} = 0.1$ was considered, which corresponds to a 50% increase in the steady-state input ($u_{SS} = 0.2$). As shown in Figure 11, the input sequence for the unconstrained controller input sequence would need to be higher than the allowed value. Thus, the MPC computed action shifts the input to satisfy the constraint. The effect of the input constraint is also seen in the states norm, which takes longer to reach the origin compared to the previous results shown on the right plot of Figure 11.

As the observer states convergence is unaffected by the input sequence, the observer error norm does not change compared to the previous result. The system and the observer estimated outputs are shown in the right plot of Figure 13. As expected, as the observer states converge to the system states, the estimated

output converges to the system output. It is possible to see that the output goes below zero, which might not be acceptable. Thus, the last simulation case considers both the input and output constraints.

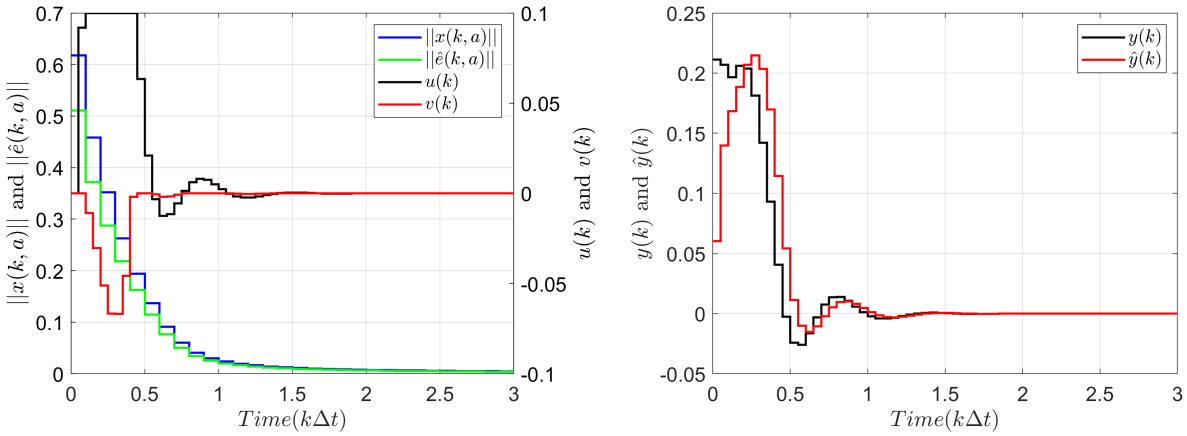

a) (Left axis) States and observer error norms; (Right axis) Total input and MPC action;

b) System output and Observer reconstructed output;

Figure 13: System and observer error norms under the control law of the Dual mode MPC considering input constraint;

The simulation results for the last case are shown in Figure 14. The same maximum input was chosen as before ($u_{max} = 0.1$) and a minimum value for the output $y_{min} = -0.001$. The control actions are different than shown in 13. The input is held as its maximum for longer than in the previous case, and after that, the MPC computed actions also increase the total input to make the output not decrease.

The observer convergence is not dependent on the control actions, and the observer error norm is the same as before. As the MPC uses the observer states (and consequently, the output), the actual output reaches lower values than the allowed minimum, as the observer states have not completely converged to the system states. This could be fixed by using an observer gain that guarantees a faster convergence, but this generally leads to a higher initial observer error. The overall effect of the constraints is also seen in the states' norm, which takes longer to reach the origin.

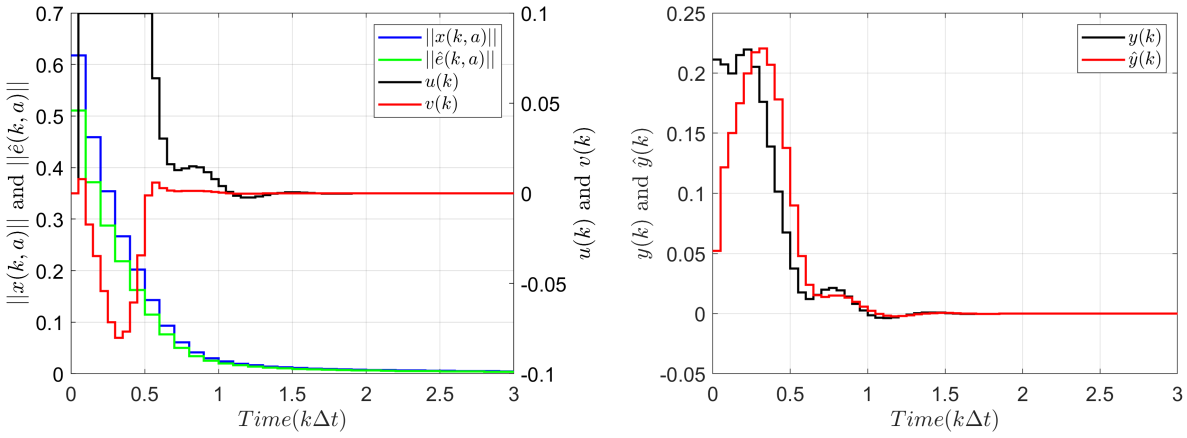

a) (Left axis) States and observer error norms; (Right axis) Total input and MPC action;

b) System output and Observer reconstructed output;

Figure 14: System and observer error norms under the control law of the Dual mode MPC considering input and output constraints;

Conclusion

The dual-mode linear model predictive controller for a scalar PIDE was designed in this work. The PIDE represents the dynamic of a population, which is usually seen in a chemostat reactor. Full-state feedback would not be possible for the type of system modeled by the PIDE, so an observer was used to reconstruct the system states. The performance of the control strategy was illustrated with numerical simulations. As the MPC considered a quadratic cost function with the same states and input costs as the stabilizing full-state feedback, the dual-mode control should not change the input given by this control law if an unconstrained system was considered, as seen in the simulation results. Lastly, when constraints are present, the MPC shifts the input given by the full-state feedback to satisfy both input and output constraints.

Acknowledgments

The support provided by CAPES - 88881.128514/2016-01 (Brazil) for Guilherme Ozorio Cassol is gratefully acknowledged.

Appendix A: Eigenfunctions and Characteristic Equation

The eigenvalue problem is given by $A\phi = \lambda\phi$. With the linear operator A defined in Eq. 16, the following ordinary integro-differential equation (OIDE) with varying coefficients is obtained:

$$\frac{d\phi}{da} = [\gamma(a) - \lambda]\phi - x_{SS}(a)\int_0^W p(\alpha)\phi d\alpha; \tag{45}$$

The Fredholm integral in this expression can initially be considered a constant, i.e., $c = \int_0^W p(\alpha)\phi d\alpha$. Thus, ϕ can be found as:

$$\phi = \mathrm{e}^{\int_0^W [\gamma(\alpha)-\lambda]d\alpha}\phi(0) - c\int_0^W x_{SS}(\alpha)\mathrm{e}^{\int_\alpha^W [\gamma(\beta)-\lambda]d\beta}d\alpha \tag{46}$$

This can be proven by taking the derivative of ϕ with respect to a:

$$\frac{d\phi}{da} = \frac{d}{da}\left(\mathrm{e}^{\int_0^W [\gamma(\alpha)-\lambda]d\alpha}\right)\phi(0) - \frac{d}{da}\left(c\int_0^W x_{SS}(\alpha)\mathrm{e}^{\int_\alpha^W [\gamma(\beta)-\lambda]d\beta}d\alpha\right) \tag{47}$$

Using Leibniz integral rule:

$$\begin{gathered}\frac{d}{da}\left(\mathrm{e}^{\int_0^W [\gamma(\alpha)-\lambda]d\alpha}\right)\phi(0) = \mathrm{e}^{\int_0^W [\gamma(\alpha)-\lambda]d\alpha}[\gamma(a)-\lambda]\phi(0) \\ \frac{d}{da}\left(\int_0^W x_{SS}(\alpha)\mathrm{e}^{\int_\alpha^W [\gamma(\beta)-\lambda]d\beta}d\alpha\right) = x_{SS}(a)c + [\gamma(a)-\lambda]c\int_0^W x_{SS}(\alpha)\mathrm{e}^{\int_\alpha^W [\gamma(\beta)-\lambda]d\beta}d\alpha\end{gathered} \tag{48}$$

Taking the first derivative and the last term of the second derivative gives:

$$\mathrm{e}^{\int_0^W [\gamma(\alpha)-\lambda]d\alpha}[\gamma(a)-\lambda]\phi(0) - [\gamma(a)-\lambda]c\int_0^W x_{SS}(\alpha)\mathrm{e}^{\int_\alpha^W [\gamma(\beta)-\lambda]d\beta}d\alpha = [\gamma(a)-\lambda]\phi \tag{49}$$

which gives the same OIDE defined in Eq. 45. It is necessary to find the value of c, the constant related to the Fredholm integral. This can be easily achieved by applying $\int_0^W p(a)(\cdot)da$ in both sides of ϕ:

$$\begin{gathered}\int_0^W p(\alpha)\phi d\alpha = c = \int_0^W p(a)\mathrm{e}^{\int_0^W [\gamma(\alpha)-\lambda]d\alpha}da\phi(0) - c\int_0^W p(a)\int_0^W x_{SS}(\alpha)\mathrm{e}^{\int_\alpha^W [\gamma(\beta)-\lambda]d\beta}d\alpha da = \\ b\phi(0) - wc \rightarrow c = \frac{b}{1+wx_{SS}}\phi(0) \rightarrow \\ \phi = \left[\mathrm{e}^{\int_0^W [\gamma(\alpha)-\lambda]d\alpha} - \frac{b}{1+wx_{SS}}\int_0^W x_{SS}(\alpha)\mathrm{e}^{\int_\alpha^W [\gamma(\beta)-\lambda]d\beta}d\alpha\right]\phi(0) = f(a)\phi(0)\end{gathered} \tag{50}$$

where b, $w(\cdot)$ and $f(a)$ were defined in Eq. 18. Finally, by applying the boundary condition, the following equation is obtained:

$$\phi(0) = \int_0^W k(a)\phi(a)da = \int_0^W k(a)f(a)da\phi(0) \rightarrow \left[1 - \int_0^W k(a)f(a)da\right]\phi(0) = 0 \tag{51}$$

and, as the trivial solution is not desired, $\phi(0) \neq 0$, the term inside the square brackets must be zero, which is the characteristic equation shown in Eq. 17.

Appendix B: Adjoint Operators

The definition of the adjoint operator is given by:

$$\langle Ax, y\rangle = \langle x, A^*y\rangle \tag{52}$$

Using the linear operator defined in Eq. 16 on the left side of the equation and the inner product defined in Eq. 20 gives:

$$\begin{gathered}\langle Ax, y\rangle = \left\langle\left[-\frac{\partial x}{\partial a} + \gamma(a)x - x_{SS}(a)\int_0^W p(\alpha)x(\alpha)d\alpha\right], y\right\rangle = \\ \int_0^W\left[-\frac{\partial x}{\partial a} + \gamma(a)x - x_{SS}(a)\int_0^W p(\alpha)x(\alpha)d\alpha\right]y(a)da\end{gathered} \tag{53}$$

For better understanding, each term is worked on separately:

$$\begin{gathered}\int_0^W \left[-\frac{\partial x}{\partial a}\right] y(a)da = \int_0^W x(a)\frac{\partial y}{\partial a}da - [x(a)y(a)]|_0^W = \int_0^W x(a)\frac{\partial y}{\partial a}da - x(W)y(W) + x(0)y(0) = \\ \int_0^W x(a)\frac{\partial y}{\partial a}da - x(W)y(W) + \int_0^W k(a)x(a)y(0)da = \int_0^W x(a)\left[\frac{\partial y}{\partial a} + k(a)y(0)\right]da - x(W)y(W)\end{gathered} \tag{54}$$

where integration by parts was used to deal with the derivative. The second term is straightforward:

$$\int_0^W [\gamma(a)x(a)]\, y(a)da = \int_0^W x(a)\,[\gamma(a)y(a)]\,da \tag{55}$$

Finally, the last term results in the following:

$$\begin{gathered}\int_0^W \left[-x_{SS}(a)\int_0^W p(\alpha)x(\alpha)d\alpha\right] y(a)da = \int_0^W \int_0^W [-x_{SS}(a)]p(\alpha)x(\alpha)y(a)d\alpha da = \\ \int_0^W \int_0^W [-x_{SS}(a)]p(\alpha)x(\alpha)y(a)da d\alpha = \int_0^W x(\alpha)\left[-p(\alpha)\int_0^W x_{SS}(a)y(a)da\right]d\alpha = \\ \int_0^W x(a)\left[-p(a)\int_0^W x_{SS}(\alpha)y(\alpha)d\alpha\right]da\end{gathered} \tag{56}$$

Thus, the adjoint operator of A will be:

$$\int_0^W x(\alpha)\left[\frac{\partial y}{\partial a} + \gamma(a)y(a) - p(a)\int_0^W x_{SS}(\alpha)y(\alpha)d\alpha + k(a)y(0)\right]d\alpha \tag{57}$$

with $y(W) = 0$. For the operators B and C, the process is repeated:

$$\begin{gathered}\langle Bu, y\rangle = \int_0^W [-x_{SS}(a)u]y(a)da = u\int_0^W [-x_{SS}(a)]y(a)da = \langle u, B^*y\rangle \\ \langle Cx, y\rangle = \left[\int_0^W x(a)da\right]y = \int_0^W x(a)yda = \langle x, C^*y\rangle\end{gathered} \tag{58}$$

which gives $B^*(\cdot) = \int_0^W [-x_{SS}(a)](\cdot)da$ and $C^* = 1$.

Appendix C: Resolvent Operator

The resolvent operator can be determined by applying Laplace Transform on the system defined on Eq. 15 and Eq. 16, which leads to the following OIDE:

$$\frac{dX}{da} = [\gamma(a) - s]X - x_{SS}(a)\int_0^W p(\alpha)Xd\alpha + x_0(a); \tag{59}$$

which is an ordinary integro-differential equation with varying coefficients. Once again, the Fredholm integral can be defined as $c = \int_0^W p(\alpha)Xd\alpha$, resulting in:

$$X = \mathrm{e}^{\int_0^W [\gamma(\alpha)-s]d\alpha}X(0) - c\int_0^W x_{SS}(\alpha)\mathrm{e}^{\int_\alpha^W [\gamma(\beta)-s]d\beta}d\alpha + \int_0^W x_0(\alpha)\mathrm{e}^{\int_\alpha^W [\gamma(\beta)-s]d\beta}d\alpha \tag{60}$$

which, similarly to what was developed in Appendix A, can be proven to be the solution of the OIDE. To find the value of c, the $\int_0^W p(a)(\cdot)da$ is applied in both sides of X:

$$\begin{gathered}\int_0^W p(\alpha)Xd\alpha = c = \int_0^W p(a)\mathrm{e}^{\int_0^W [\gamma(\alpha)-s]d\alpha}daX(0) \\ -c\int_0^W p(a)\int_0^W x_{SS}(\alpha)\mathrm{e}^{\int_\alpha^W [\gamma(\beta)-s]d\beta}d\alpha da + \int_0^W p(a)\int_0^W x_0(\alpha)\mathrm{e}^{\int_\alpha^W [\gamma(\beta)-s]d\beta}d\alpha sa = \\ bX(0) - wx_{SS}c + wx_0 \to c = \frac{b}{1+wx_{SS}}X(0) + \frac{wx_0}{1+wx_{SS}} \to \\ X = \left[\mathrm{e}^{\int_0^W [\gamma(\alpha)-s]d\alpha} - \frac{b}{1+wx_{SS}}\int_0^W x_{SS}(\alpha)\mathrm{e}^{\int_\alpha^W [\gamma(\beta)-s]d\beta}d\alpha\right]X(0) \\ -\frac{wx_0}{1+wx_{SS}}\int_0^W x_{SS}(\alpha)\mathrm{e}^{\int_\alpha^W [\gamma(\beta)-s]d\beta}d\alpha + \int_0^W x_0(\alpha)\mathrm{e}^{\int_\alpha^W [\gamma(\beta)-s]d\beta}d\alpha = f(a)X(0) + \Omega x_0\end{gathered} \tag{61}$$

where b, $w(\cdot)$ and $f(a)$ were defined in Eq. 18 and $\Omega(\cdot)$ on Eq. 25. The last step is to apply the boundary condition to find $X(0)$:

$$X(0) = \int_0^W k(a)X(a)da = \int_0^W k(a)f(a)daX(0) + \int_0^W k(a)\Omega x_0 da \rightarrow X(0) = \frac{\int_0^W k(a)\Omega x_0 da}{1 - \int_0^W k(a)f(a)da} \quad (62)$$

and, by substituting this in Eq. 61 the resolvent operator defined in Eq. 24 is obtained.

Appendix D: Solution of the Ricatti Equation for the Full state Feedback

As shown in Curtain[22], Eq. 30 can also be written as:

$$< \bar{Q}_C x_1, Ax_2 > + < Ax_1, \bar{Q}_C x_2 > - < R^{-1}B^*\bar{Q}_C x_1, B^*\bar{Q}_C x_2 >= - < Q_C x_1, x_2 > \quad (63)$$

for $x_1, x_2 \in \mathcal{X}$. The solution of this Ricatti equation can be written as an operator in the bi-orthogonal basis of A_d (which has the same eigenfunctions of A), such that $\bar{Q}_C x = \sum_i \sum_j q^C_{ij} < x, \bar{\psi}_i > \bar{\psi}_j$. By setting $x_1 = \phi_N$ and $x_2 = \phi_M$, the following is obtained:

$$\begin{gathered}
A_d x_1 = A_d\phi_N = \lambda^D_N \phi_N \,\&\, A_d x_2 = A_d\phi_M = \lambda^D_M\phi_M \\
\bar{Q}_C x_1 = \bar{Q}_C\phi_N = \textstyle\sum_j q^c_{N,j}\bar{\psi}_j \,\&\, \bar{Q}_C x_2 = \bar{Q}_C\phi_M = \sum_j q^c_{M,j}\bar{\psi}_j \\
\bar{Q}_C A_d x_1 = \bar{Q}_C A_d\phi_N = \textstyle\sum_j q^c_{N,j}\lambda^D_N\bar{\psi}_j \,\&\, \bar{Q}_C A_d x_2 = \bar{Q}_C A_d\phi_M = \sum_j q^c_{M,j}\lambda^D_M\bar{\psi}_j \\
B^*_d\bar{Q}_C A_d x_1 = B^*_d\bar{Q}_C\lambda^D_N\phi_N = \textstyle\sum_j q^c_{N,j}\lambda^D_N B^*_d\bar{\psi}_j \,\&\, B^*_d\bar{Q}_C A_d x_2 = B^*_d\bar{Q}_C\lambda^D_M\phi_M = \sum_j q^c_{M,j}\lambda^D_M B^*_d\bar{\psi}_j \\
B^*_d\bar{Q}_C B_d = \textstyle\sum_i\sum_j q^c_{i,j} < B_d, \bar{\psi}_i > B^*_d\bar{\psi}_j = \sum_i\sum_j q^c_{i,j} < 1, B^*_d\bar{\psi}_i > B^*_d\bar{\psi}_j
\end{gathered} \quad (64)$$

Thus, for each term on the Ricatti equation, we have:

$$\begin{gathered}
\left\langle A_d x_1, \bar{Q}_C A_d x_2\right\rangle = \left\langle \lambda^D_N\phi_N, \textstyle\sum_j q^c_{M,j}\lambda^D_M\psi_j\right\rangle = \lambda^D_N q^c_{N,M}\lambda^D_M \\
\left\langle x_1, \bar{Q}_C x_2\right\rangle = \left\langle \phi_N, \textstyle\sum_j q^c_{M,j}\psi_j\right\rangle = q^c_{N,M} \\
\left\langle (B^*_d\bar{Q}_C A_d)x_1, (R + B^*_d\bar{Q}_C B_d)^{-1}(B^*_d\bar{Q}_C A_d)x_2\right\rangle = \\
\left\langle \lambda^D_N\textstyle\sum_j q^c_{N,j}B^*_d\psi_j, (R + \sum_i\sum_j q^c_{i,j} < 1, B^*_d\psi_i > B^*_d\psi_j)^{-1}\sum_j q^c_{M,j}\lambda^D_M B^*_d\psi_j\right\rangle \\
\langle x_1, Q_C x_2\rangle = \langle \phi_N, Q_C\phi_M\rangle
\end{gathered} \quad (65)$$

where the fact that $\bar{q}^c_{M,N} = q^c_{N,M}$ was used. Finally, the Ricatti equation can be written as:

$$\begin{gathered}
\lambda^D_N q^c_{N,M}\lambda^D_M - q^c_{N,M} - (\lambda^D_N\textstyle\sum_j q^c_{N,j}b_j)^T(R + \sum_i\sum_j b^*_i q^c_{i,j}b_j)^{-1}\overline{\lambda}^D_M(\sum_j q^c_{M,j}b_j = \\
-(\psi_N)^T Q_C\overline{\psi_M}
\end{gathered} \quad (66)$$

Appendix E: Solution of the Ricatti Equation for the Observer Design

From [22], Eq. 36 can also be written as:

$$\begin{gathered}
< \bar{Q}_O A^*_d x_1, A^*_d x_2 > - < \bar{Q}_O x_1, x_2 > - < (I + C_{m,d}\bar{Q}_O C^*_{m,d})^{-1}C_{m,d}\bar{Q}_O A^*_d x_1, C_{m,d}\bar{Q}_O A^*_d x_2 >= \\
- < Q_O C_{m,d}x_1, C_{m,d}x_2 >
\end{gathered} \quad (67)$$

for $x_1, x_2 \in \mathcal{X}^*$. By defining the operator in the bi-orthogonal basis of A_d (which has the same eigenfunctions of A), we have $\bar{Q}_O(\cdot) = \sum_i \sum_j q^o_{i,j} < \phi_i, (\cdot) > \phi_j$ and taking $x_1 = \bar{\psi}_N$ and $x_2 = \bar{\psi}_M$, leads to:

$$\begin{gathered}
A^*_d x_1 = A^*_d \bar{\psi}_N = \bar{\lambda}^D_N \bar{\psi}_N \,\&\, A^*_d x_2 = A^*_d \bar{\psi}_M = \bar{\lambda}^D_M \bar{\psi}_M \\
\bar{Q}_O x_1 = \bar{Q}_O \bar{\psi}_N = \textstyle\sum_j q^o_{N,j} \phi_j \,\&\, \bar{Q}_O x_2 = \bar{Q}_O \bar{\psi}_M = \sum_j q^o_{M,j} \phi_j \\
A_d \bar{Q}_O x_1 = A_d \bar{Q}_O \bar{\psi}_N = \textstyle\sum_j q^o_{N,j} \lambda^D_j \phi_j \,\&\, A_d \bar{Q}_O x_2 = A_d \bar{Q}_O \bar{\psi}_M = \sum_j q^o_{M,j} \lambda^D_j \phi_j \\
C_m \bar{Q}_O A^*_d x_1 = C_m \bar{Q}_O \bar{\lambda}^D_N \bar{\psi}_N = \textstyle\sum_j q^o_{N,j} \lambda^D_N C_m \phi_j \,\&\, C_m \bar{Q}_O A^*_d x_2 = C_m \bar{Q}_O \bar{\lambda}^D_M \bar{\psi}_M = \sum_j q^o_{M,j} \lambda^D_M C_m \phi_j \\
C_{m,d} \bar{Q}_O C^*_{m,d} = \textstyle\sum_i \sum_j q^o_{i,j} < \phi_i, C^*_{m,d} > C_{m,d} \phi_j = \sum_i \sum_j q^o_{i,j} < C_{m,d} \phi_i, 1 > C_{m,d} \phi_j
\end{gathered} \tag{68}$$

where the properties of the inner product and the bi-orthogonal shown in the previous sections were used. Going back to Eq. 67:

$$\begin{gathered}
< \textstyle\sum_j q^o_{N,j} \lambda^D_j \phi_j, \bar{\lambda}^D_M \bar{\psi}_M > - < \sum_j q^o_{N,j} \phi_j, \psi_M > \\
- < (I + \textstyle\sum_i \sum_j q^o_{i,j} < C_{m,d} \phi_i, 1 > C_{m,d} \phi_j)^{-1} \sum_j q^o_{N,j} \lambda^D_N C_m, \sum_j q^o_{M,j} \lambda^D_M C_m >= \\
- < Q_O C_{m,d} \bar{\psi}_N, C_{m,d} \bar{\psi}_M > \rightarrow \\
< \textstyle\sum_j q^o_{N,j} \lambda_j \phi_j, \psi_M > + < \psi_N, \sum_j q^o_{M,j} \lambda_j \phi_j > - < \sum_j q^o_{N,j} C_m \phi_j, \sum_j q^o_{M,j} C_m \phi_j >= \\
- < C_m x_1, Q_O C_m x_2 > \rightarrow \\
q^o_{N,M} \lambda_M + q^o_{N,M} \bar{\lambda}_N - (C_m \Phi q^o_{N,:})^T \overline{(C_m \Phi q^o_{M,:})} = -(C_m \psi_N)^T Q_O \overline{(C_m \psi_M)}
\end{gathered} \tag{69}$$

where $q_{N,M} = \bar{q}_{M,N}$ was used.

References

1. H. L. Smith, P. Waltman, The Theory of the Chemostat: Dynamics of Microbial Competition, Cambridge Studies in Mathematical Biology, Cambridge University Press, 1995.

2. D. Toth, M. Kot, Limit cycles in a chemostat model for a single species with age structure, Mathematical Biosciences 202 (1) (2006) 194–217.

3. F. Brauer, Mathematical models in population biology and epidemiology / Fred Brauer, Carlos Castillo-Chavez., Texts in applied mathematics; 40, Springer, 2001.

4. U. Badillo-Hernandez, J. Alvarez, L. Alvarez-Icaza, Efficient modeling of the nonlinear dynamics of tubular heterogeneous reactors, Computers & Chemical Engineering 123 (2019) 389–406.

5. M. J. Balas, Feedback control of linear diffusion processes, International Journal of Control 29 (3) (1979) 523–534.

6. W. H. Ray, Advanced process control., New York McGraw-Hill, 1981.

7. J. Deutscher, N. Gehring, R. Kern, Output feedback control of general linear heterodirectional hyperbolic ode–pde–ode systems, Automatica 95 (2018) 472 – 480.

8. P. Christofides, P. Daoutidis, Finite-dimensional control of parabolic pde systems using approximate inertial manifolds, Journal of Mathematical Analysis and Applications 216 (2) (1997) 398–420.

9. I. Aksikas, J. J. Winkin, D. Dochain, Optimal LQ-feedback regulation of a nonisothermal plug flow reactor model by spectral factorization, IEEE Transactions on Automatic Control 52 (7) (2007) 1179–1193.

10. I. Aksikas, A. A. Moghadam, J. F. Forbes, Optimal linear–quadratic control of coupled parabolic–hyperbolic pdes, International Journal of Control 90 (10) (2017) 2152–2164.

11. I. Karafyllis, M. Malisoff, M. Krstic, Sampled-data feedback stabilization of age-structured chemostat models, in: 2015 American Control Conference (ACC), 2015, pp. 4549–4554.

12. K. Schmidt, I. Karafyllis, M. Krstic, Yield trajectory tracking for hyperbolic age-structured population systems, Automatica 90 (2018) 138–146.

13. I. Karafyllis, M. Krstic, On the relation of delay equations to first-order hyperbolic partial differential equations, ESAIM: Control, Optimisation and Calculus of Variations 20 (3) (2014) 894–923.

14. K. R. Muske, J. B. Rawlings, Model predictive control with linear models, AIChE Journal 39 (2) (1993) 262–287.

15. P. Dufour, Y. Touré, D. Blanc, P. Laurent, On nonlinear distributed parameter model predictive control strategy: on-line calculation time reduction and application to an experimental drying process, Computers & Chemical Engineering 27.

16. S. Dubljevic, P. D. Christofides, Predictive control of parabolic pdes with boundary control actuation, Chemical Engineering Science 61 (18) (2006) 6239 – 6248.

17. A. Armaou, A. Ataei, Piece-wise constant predictive feedback control of nonlinear systems, Journal of Process Control 24 (4) (2014) 326 – 335.

18. L. C. Hairer E., G. Wanner, Geometric Numerical Integration: Structure-Preserving Algorithms for Ordinary Differential Equations, Vol. 31 of Springer Series in Computational Mathematics, Springer, Berlin, 2002.

19. V. Havu, J. Malinen, The Cayley transform as a time discretization scheme, Numerical Functional Analysis and Optimization 28 (7-8) (2007) 825–851.

20. Q. Xu, S. Dubljevic, Linear Model Predictive Control for Transport-Reaction Processes, AIChE Journal 63 (7).

21. S. Dubljevic, J.-P. Humaloja, Model predictive control for regular linear systems, Automatica 119 (2020) 109066.

22. R. F. Curtain, H. Zwart, An introduction to Infinite-Dimensional Linear Systems Theory, Springer-Verlag, New York, 1995.